Electronic Supplementary Material (ESI) for Journal of Materials Chemistry A.

Supporting Information

Three-dimensional CoOOH Nanoframes Confining High-density Mo Single Atoms for Large-current-density Oxygen Evolution

Lei Tang[1,2†], Liang Yu[1,2†], Chao Ma[3], Yao Song[1,2], Yunchuan Tu[1,2], Yunlong Zhang[1,2], Xin Bo[1,2] and Dehui Deng[1,2*]

[1]State Key Laboratory of Catalysis, Dalian Institute of Chemical Physics, Chinese Academy of Sciences, Zhongshan Road 457, Dalian 116023, China

[2]University of Chinese Academy of Sciences, Beijing 100049, China

[3]College of Materials Science and Engineering, Hunan University, Changsha 410082, China

*Email: dhdeng@dicp.ac.cn

1, Chemicals

The following chemicals were used in this work, including cobalt nitrate hexahydrate ($Co(NO_3)_2$•$6H_2O$, 99.0%, Sigma-Aldrich), 2-methylimidzole (MIM, 99%, Sigma-Aldrich), sodiummolybdate dihydrate (Na_2MoO_4, 99.0%, Tianjin Guangfu Company), Sodium tungstate dihydrate (Na_2WO_4, 99.0%, Tianjin Guangfu Company), Ethanol (Tianjin Guangfu Fine Chemical Research Institute), Nafion solution (~5 wt.%, Sigma-Aldrich). All the chemicals are reagent-grade and used as received. High-purity water (18.25 mΩ·cm) supplied by a UP Water Purification System was used in all the experiments.

2, Methods

Synthesis of ZIF-67. ZIF-67 were prepared on the basis of a previously reported method. In a typical synthesis, 59 mg of $Co(NO_3)_2·6H_2O$ and 1.6 mg of cetrimonium bromide (CTAB) were fully dissolved in 2 ml of deionized water to form a clear solution. Then, the solution was rapidly added into 14 ml of aqueous solution containing 908 mg of 2-methylimidazole with magnetic stirring at room temperature for 20 min. The purple precipitates were centrifuged, washed with ethanol and dried at 80 °C for overnight.

Synthesis of Mo-CoOOH. ZIF-67 as self-templates were topologically converted into Mo-CoOOH by adding Na_2MoO_4 into the reaction solution. In detail, the above obtained ZIF-67 products were redispersed in 30 mL of ethanol, which was then added into 20 mL of deionized water containing 50 mg of Na_2MoO_4. Thereafter, the mixtures were transferred into a round-bottom flask and refluxed at 82 °C for 2 h. The formed Mo-CoOOH was centrifuged and washed with ethanol for several times, then the products were dried before use. Further increasing the loading of Mo leads to the stacking of the Mo-CoOOH layer and thus are not considered (Supplementary Figure 23). In addition, the synthetic procedure of pure CoOOH was similar with that of Mo-CoOOH, except that urea was used instead of Na_2MoO_4.

Synthesis of W-CoOOH. The synthetic procedure of W-CoOOH was similar with that of Mo-CoOOH, except that Na_2WO_4 (68 mg) was used instead of Na_2MoO_4.

Material characterizations. We characterized the structures and morphologies of the synthesized materials by a HT7700 transmission electron microscope (TEM) and a JEM-F200 TEM and obtained the elemental maps by JEOL JEM-2100F field emission electron microscope. Aberration-corrected scanning transmission electron microscopy characterizations were conducted by a JEOL ARM200F microscope equipped with a probe-forming aberration corrector, which was operated at 200 kV. We analyzed the crystalline structure and phase purity by X'pert Pro-1 X-ray diffraction (XRD) with Cu Kα radiation source. We investigated the metal concentration of the Co-based oxyhydroxides by inductively coupled plasma optical emission spectrometry (ICP-OES) in IRIS Intrepid II XSP (Thermo ELECTRON). The N_2 adsorption-desorption isotherms were measured using a Micromeritics Tristar 3020 Surface Area and Porosimetry analyzer at liquid-nitrogen temperature. Operando Raman spectroscopy was performed on LabRAM HR 800 Raman spectrometer

with 532 nm laser excitation. A Thermo Fisher Nicolet IS50 spectrometer equipped with the MCT detector and a Pike Technologies VeeMAX Ⅲ ATR accessory was employed for the operando ATR-IR measurements.

XAFS measurements. X-ray absorption fine structure spectroscopy (XAFS) measurements at the Co K-edge were performed in the transmission mode with the Si (111) monochromator at BL14W1 station in Shanghai Synchrotron Radiation Facility, China. The storage rings of SSRF were operated at 3.5GeV with a maximum current of 210 mA. XAFS measurements at the Mo K-edge and W L_3-edge were performed in the transmission mode with the Si (311) monochromator at BL14W1 station in Shanghai Synchrotron Radiation Facility, China. The storage rings of SSRF were operated at 3.5 GeV with a maximum current of 210 mA.

Electrochemical measurements. All of the electrochemical measurements were performed on an electrochemical workstation (PARSTAT 2273 potentiostat/galvanostat) in a three-electrode system with 1M KOH solution as the electrolyte, Pt mesh as the counter electrode and Hg/HgO (1 M KOH solution) as the reference electrode. The glassy carbon rotating disk electrode with a diameter of 5 mm loaded with various catalysts was used as the working electrode. Typically, 4 mg of catalyst, 2 mg XC-72 and 25 μl of Nafion solution (5 wt%, Du Pont) were suspended in 1 ml ethanol to form a homogeneous ink assisted by ultrasound. Then 25 μL of the ink was drop-casted onto the surface of glassy carbon electrode and dried under room temperature. The electrochemical measurements were conducted by using rotating disk electrode (RDE) in O_2-saturated 1 M KOH electrolyte at 25 °C with a scan rate of 5 mV s^{-1} under 1600 rpm. Before the linear sweep voltammetry (LSV) test, the catalysts were repeatedly swept from -0.5 V to 0 V in KOH solution until a steady voltammogram curve was obtained.

The OER performances of the Mo-CoOOH and IrO_2 at large current densities were measured by coating the catalysts on Ni foam electrodes. The electrochemical measurements were conducted in a standard three-electrode system. Hg/HgO electrode and Pt mesh were used as the reference and counter electrodes, respectively. For the preparation of the working electrode, 4 mg Mo-CoOOH were suspended in 1 mL ethanol with 25 μL Nafion solution to form a homogeneous ink. Then, this ink was dropped on Ni foam (1 cm × 1 cm). In the electrochemical stability test, a sample injector containing pure water is used to continuously replenish water to avoid the change of electrolyte concentration. For the conversion of potential to be versus the reversible hydrogen electrode (RHE), the Hg/HgO reference electrode was calibrated in H_2-saturated 1 M KOH solution by measuring hydrogen oxidation/evolution at a platinum mesh electrode (Supplementary Figure 24).

The performances tested under industrial conditions were done on Ni foam at 1M KOH solution with a temperature of 85 °C. The industrial-scale measurements were carried out in an electrolyser equipped with HoAM Grion 1204 anion membrane. A 3×3 cm^2 Mo-CoOOH electrode and 20% Pt/C electrode were used as anode and cathode, respectively. A commercial precious IrO_2 electrode was used as a control.

The turnover frequency (TOF) is calculated as TOF = $\frac{jS}{4Fn}$, where j is the measured current density (mA cm^{-2}), S is the surface area of the GC electrode, the number 4 is the total number of electrons required for generating one O_2 molecule, F is the Faraday's constant (96485.3 C mol^{-1}), and n is the moles of considered metal atoms in the sample loaded on the electrode.[12]

Computational methods. Density functional theory (DFT) calculations were conducted with the projector augmented-wave pseudopotential method and Perdew-Burke-Ernzerhof (PBE) exchange-correlation functionals as implemented in the Vienna Ab-initio Simulation Package (VASP).[1-8] A plane-wave cutoff energy of 400 eV was adopted for electronic structure calculations. Van der Waals interaction was included in optimizing the structures using Zero-damping DFT-D3 method of Grimme.[9, 10] The basal planes of CoOOH, NiCoOOH, NiFeOOH, and CoFeOOH confining Mo or W atoms were simulated in 6×6 supercells. The edges of CoOOH, Mo-CoOOH, and W-CoOOH were simulated with nanoribbon models with 4 repeated units along the axial direction. The vacuum thicknesses were set larger than 15 angstroms. Monkhorst-Pack k-point samplings of 3×3×1 and 1×3×1 were selected for the two-dimensional and nanoribbon models, respectively.[11] Dipole correction was applied to decouple the interactions between the slabs or nanoribbons. The convergence criterion of forces between atoms in the structural optimization was set below 0.02 eV/Å. The free energy (G) was calculated as E_{total} + ZPE – *TS*, where E_{total} is DFT-calculated total energy, ZPE is the zero-point energy, *T* is temperature, and *S* is the entropy. The free energy of ($H^+ + e^-$) was calculated as that of $^1/_2$ H_2 under standard conditions. The free energy of ($OH^- - e^-$) was calculated based on the equilibrium of reaction ($H^+ + OH^- \rightarrow H_2O$). The free energy of O_2 was calculated as 2 $G(H_2O)$ – 2 $G(H_2)$ – 4.92 eV.

3, Supplementary Figures

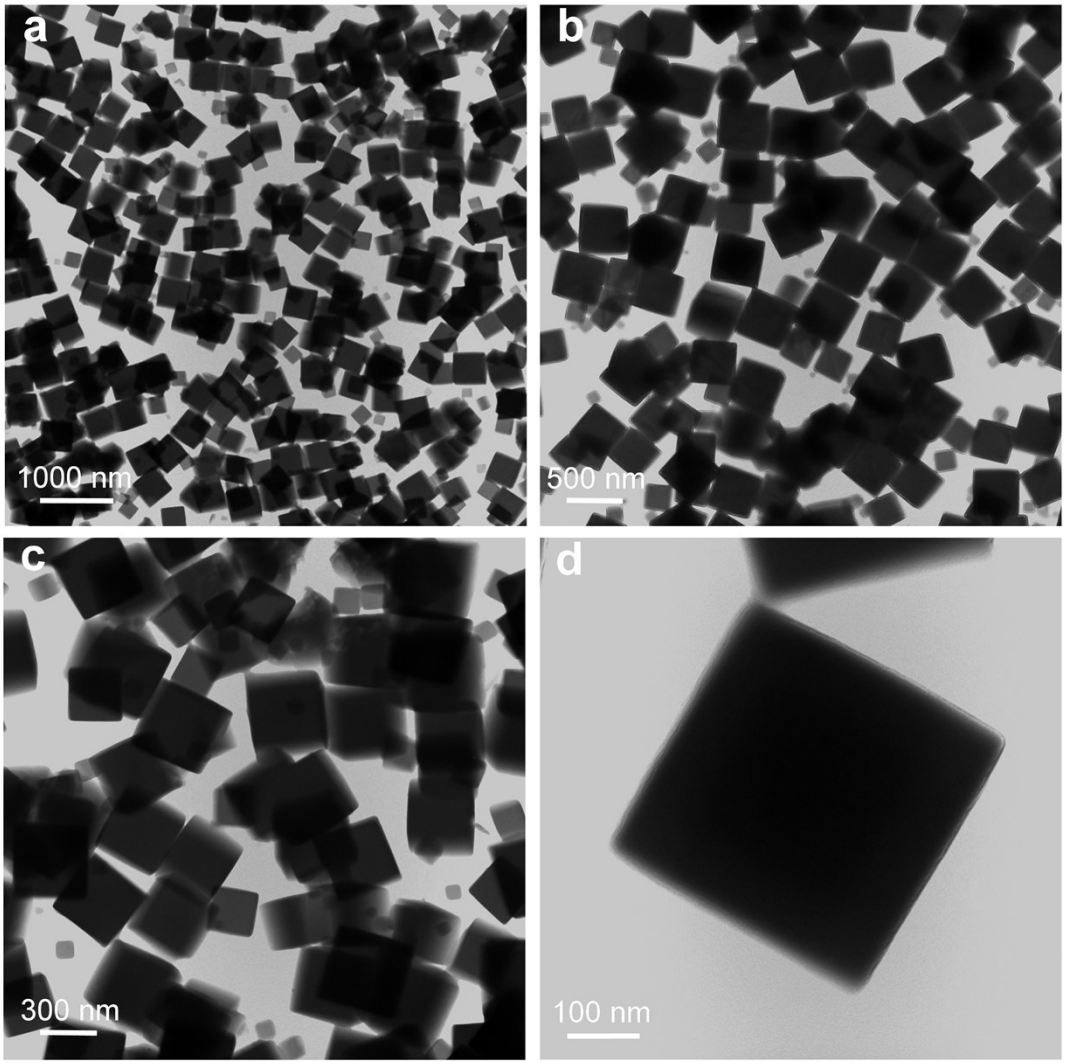

Supplementary Figure 1. (a, b, c, d) The transmission electron microscopy (TEM) images of the ZIF-67 at different size scales.

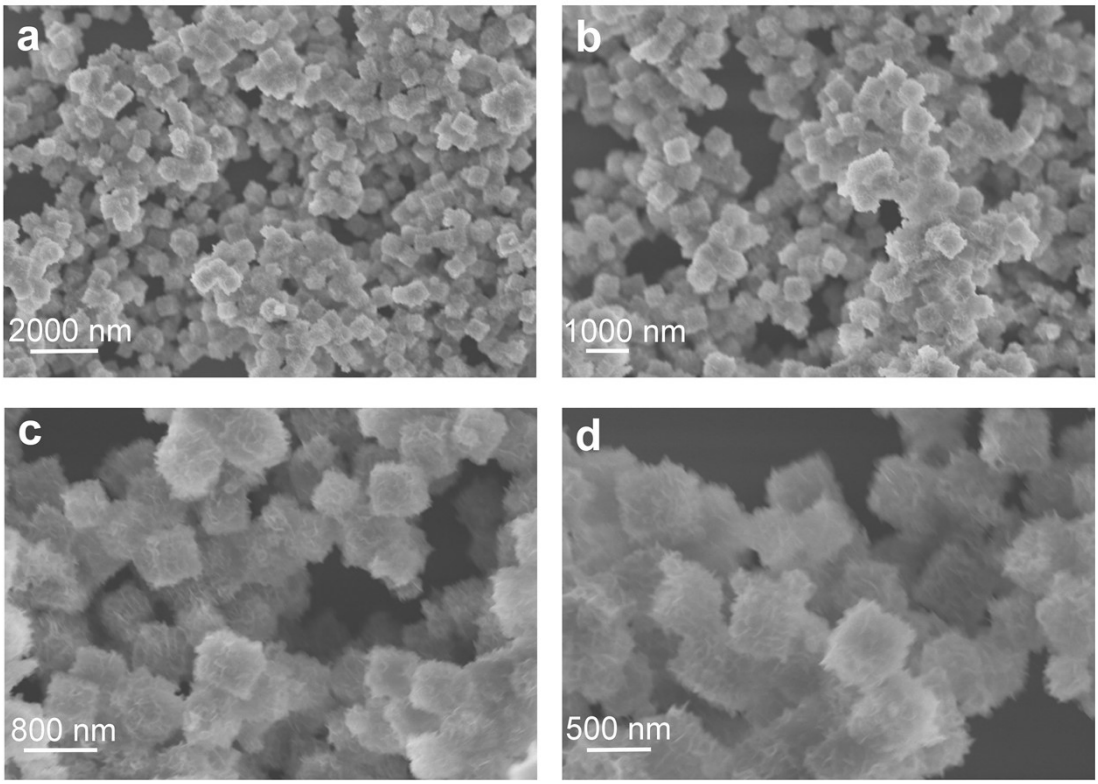

Supplementary Figure 2. (a, b, c, d) The scanning electron microscope (SEM) images of the Mo-CoOOH at different size scales.

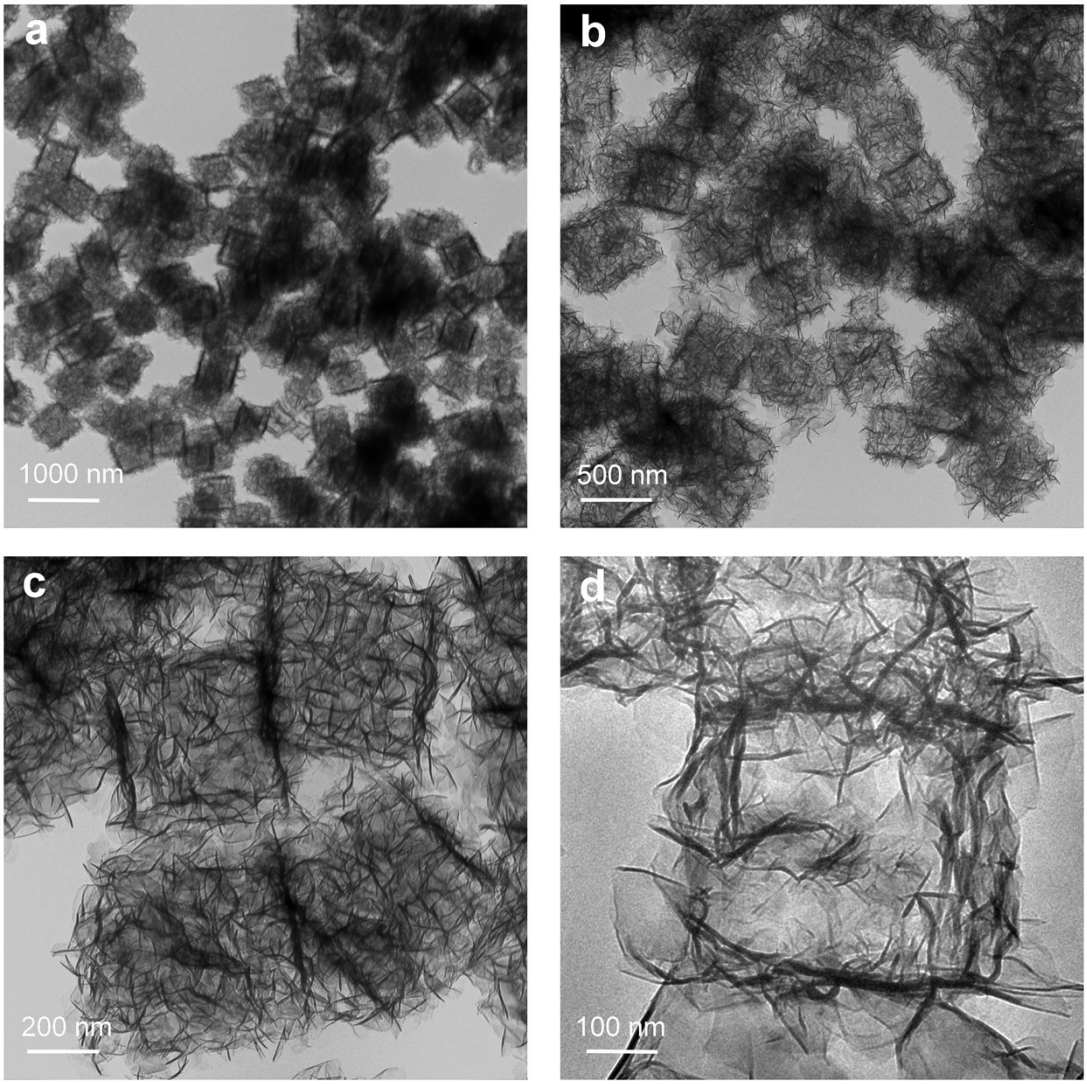

Supplementary Figure 3. (a, b, c, d) The transmission electron microscopy (TEM) images of the Mo-CoOOH at different size scales.

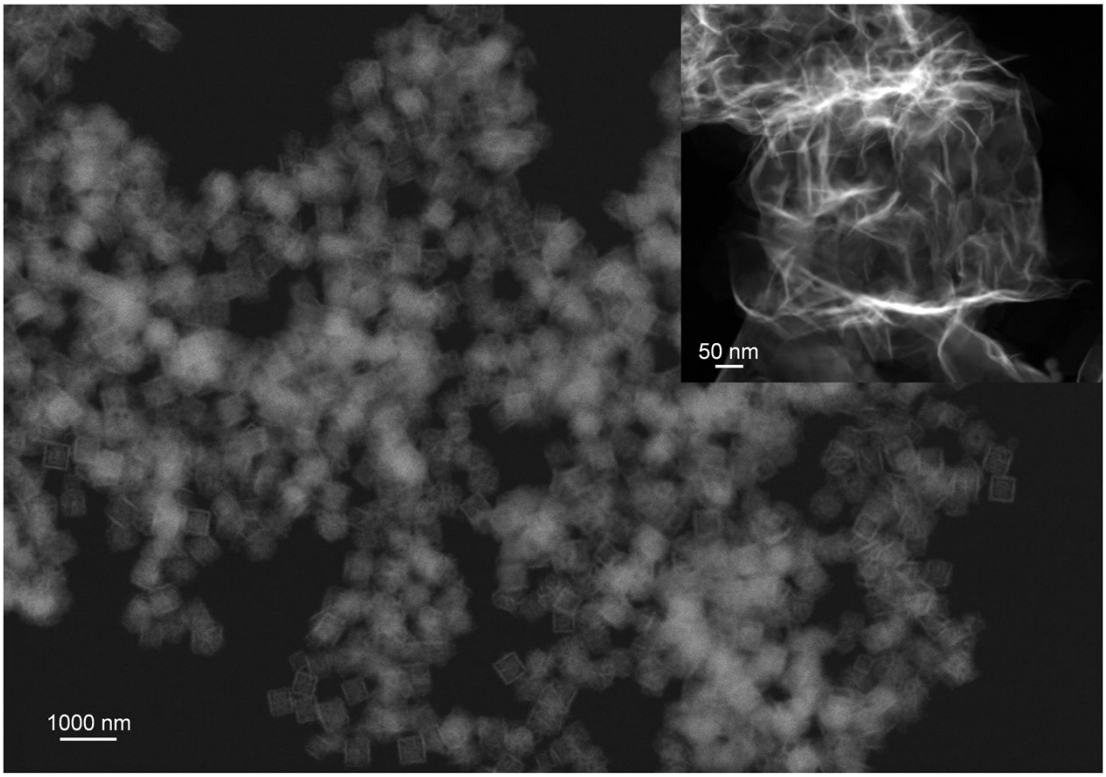

Supplementary Figure 4. The high-angle annular dark-field scanning TEM (HAADF-STEM) image of the Mo-CoOOH. The inset image shows the morphology of a typical Mo-CoOOH nanoframe.

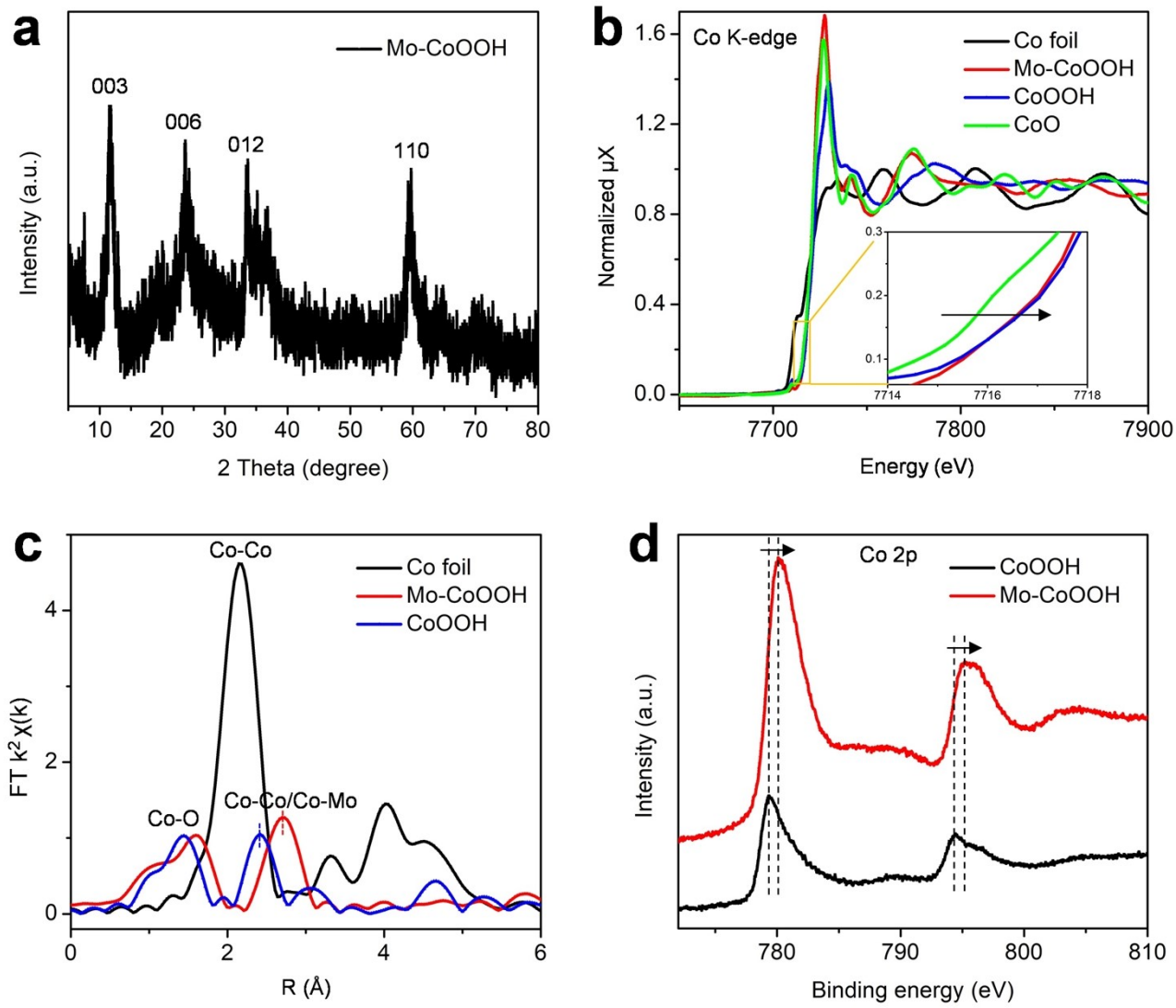

Supplementary Figure 5. (a) XRD patterns of the Mo-CoOOH. **(b)** Co K-edge XAFS spectra of the Mo-CoOOH, Co foil, CoOOH, and CoO. **(c)** k^2-weighted Fourier transformation of the Co K-edge EXAFS spectra. **(d)** XPS spectra of Co 2p for the Mo-CoOOH and the pristine CoOOH.

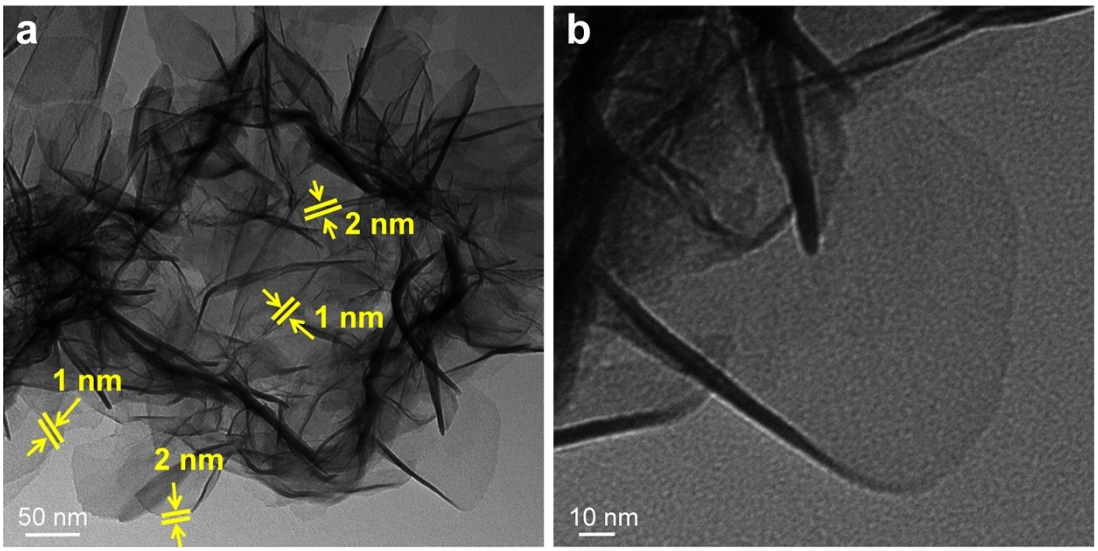

Supplementary Figure 6. The high-resolution transmission electron microscopy (HRTEM) images of the Mo-CoOOH.

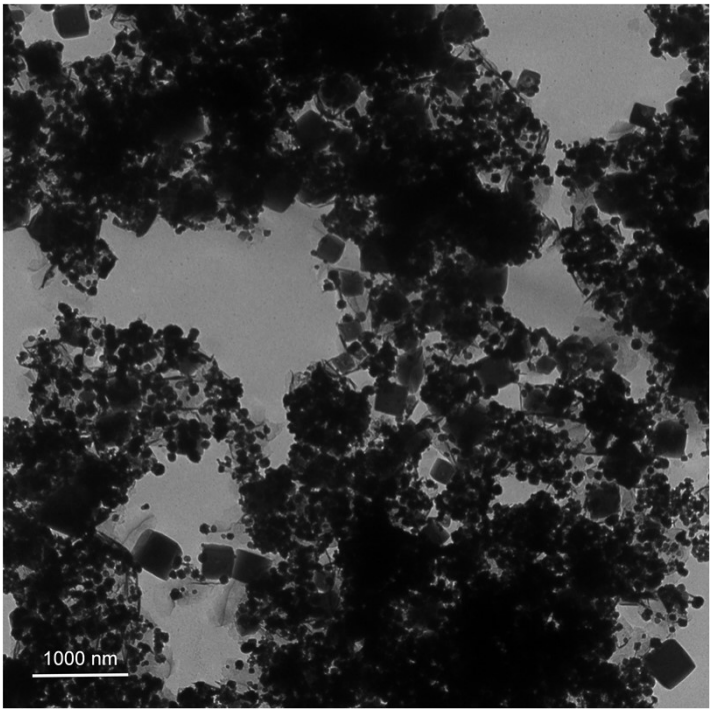

Supplementary Figure 7. The transmission electron microscopy (TEM) image of the Mo-CoOOH synthesized without adding H_2O.

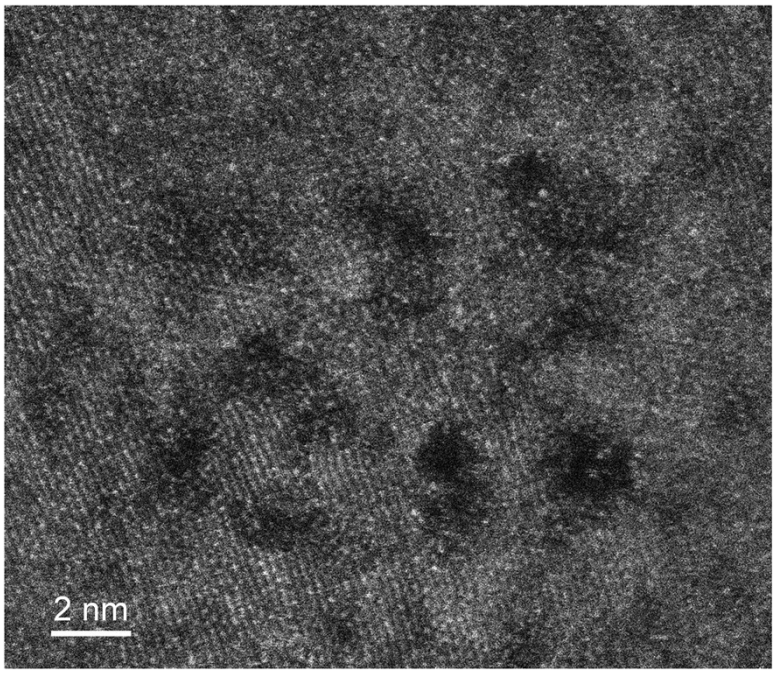

Supplementary Figure 8. Atomic-resolution high-angle annular dark-field scanning TEM (HAADF-STEM) image of the Mo-CoOOH.

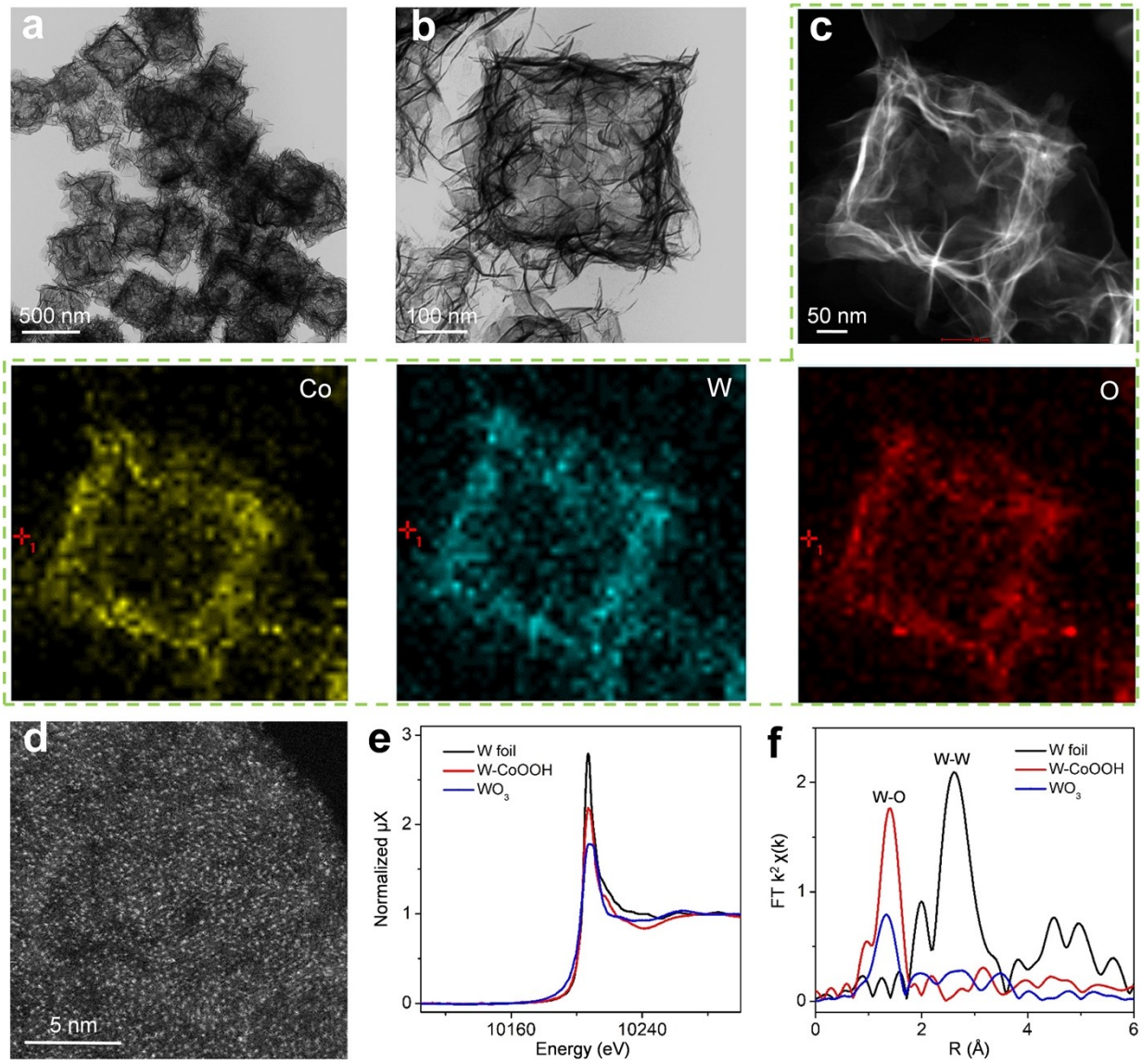

Supplementary Figure 9. (a, b) TEM images of the W-CoOOH. **(c)** X-ray energy-dispersive spectroscopy (EDS) elemental mapping results of a W-CoOOH nanoframe. **(d)** Atomic-resolution HAADF-STEM image of the W-CoOOH nanosheet. **(e)** W L_3-edge XAFS spectra of the W-CoOOH, W foil and WO_3. **(f)** k^2-weighted Fourier transformation of the W L_3-edge EXAFS spectra.

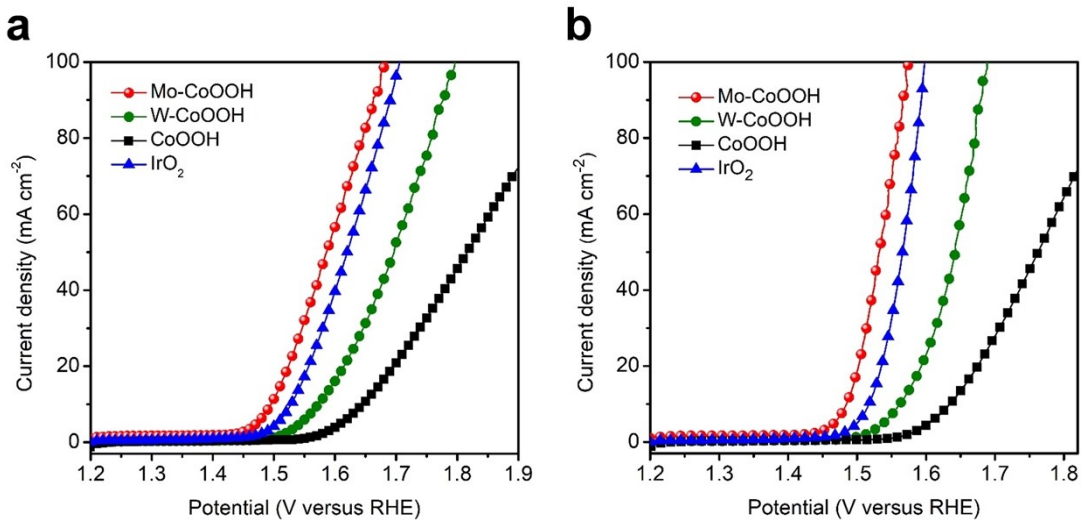

Supplementary Figure 10. The OER polarization curves of catalysts loaded on glassy carbon electrode, without iR corrections **(a)** and with 90% iR corrections **(b)**.

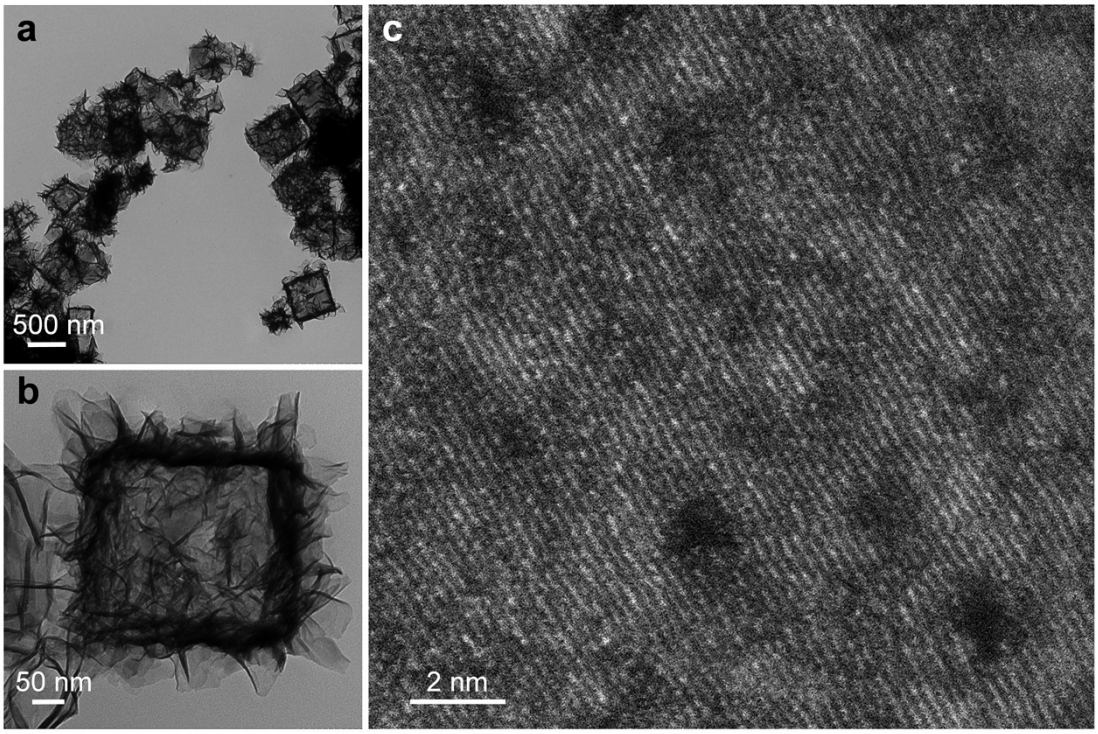

Supplementary Figure 11. (a, b) TEM images of the Mo-CoOOH nanoframes after OER stability test of 36 hours at 10 mA cm^{-2}, showing that the morphology of the nanoframes can be well maintained after the reaction. **(c)** Atomic-resolution HAADF-STEM image of the Mo-CoOOH after the OER stability test of 36 hours at 10 mA cm^{-2}.

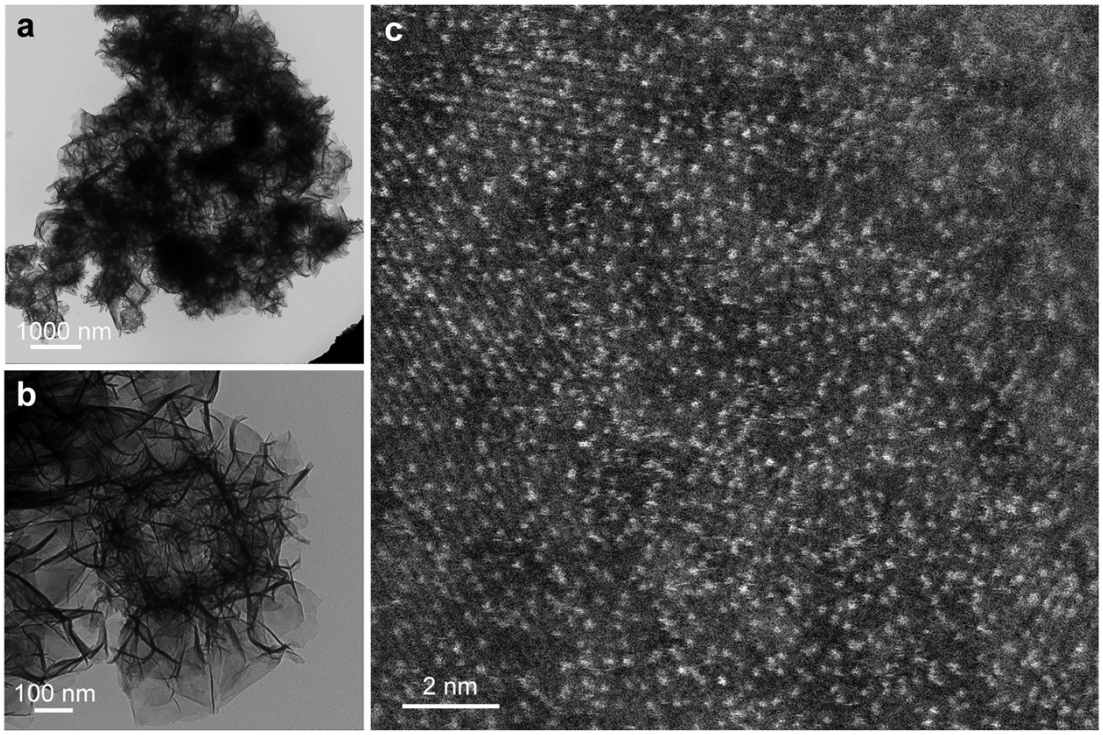

Supplementary Figure 12. (a, b) TEM images of the W-CoOOH nanoframes after OER stability test of 36 hours at 10 mA cm^{-2}, showing that the morphology of the nanoframes can be well maintained after the reaction. **(c)** Atomic-resolution HAADF-STEM image of the W-CoOOH after the OER stability test of 36 hours at 10 mA cm^{-2}.

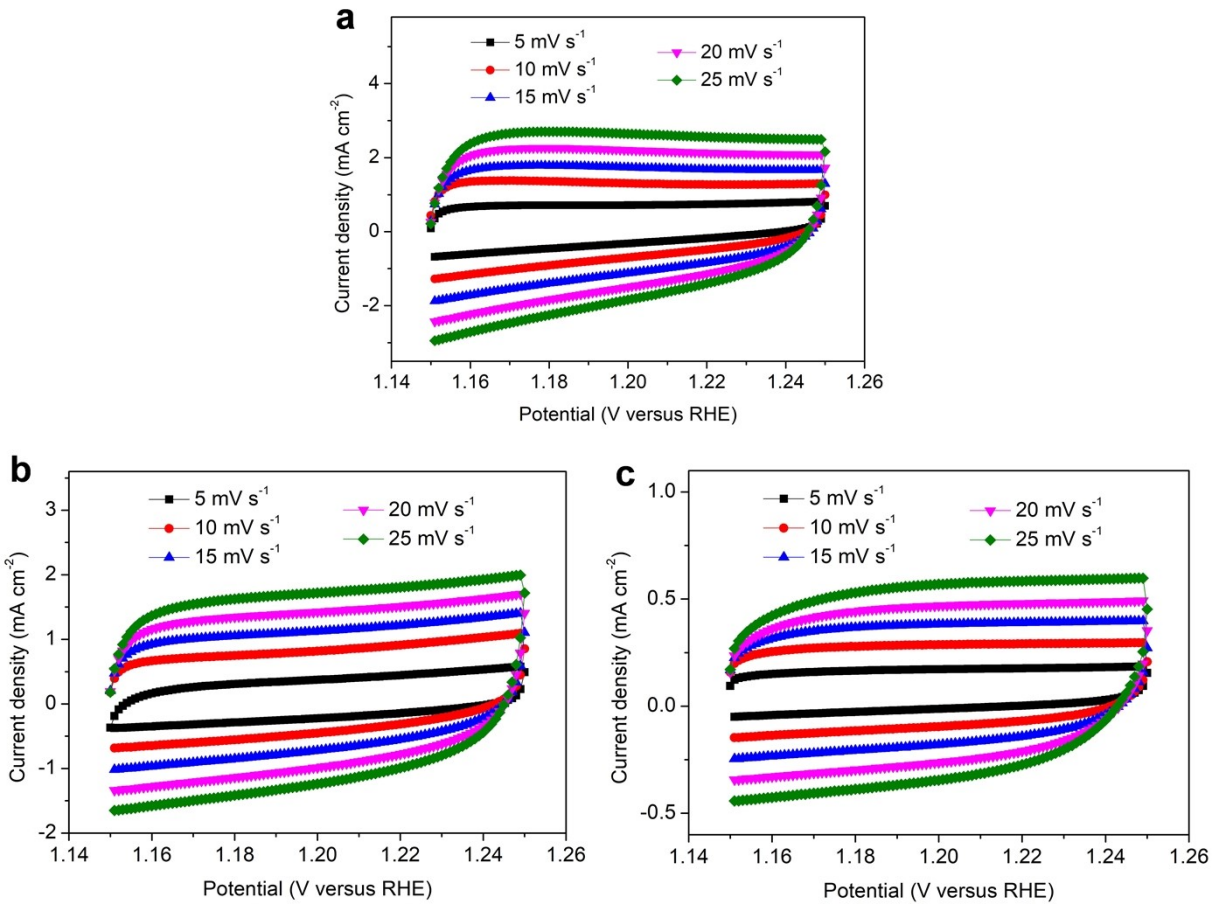

Supplementary Figure 13. Cyclic voltammetry curves over the Mo-CoOOH **(a)**, W-CoOOH **(b)**, and CoOOH **(c)** at different scan rates.

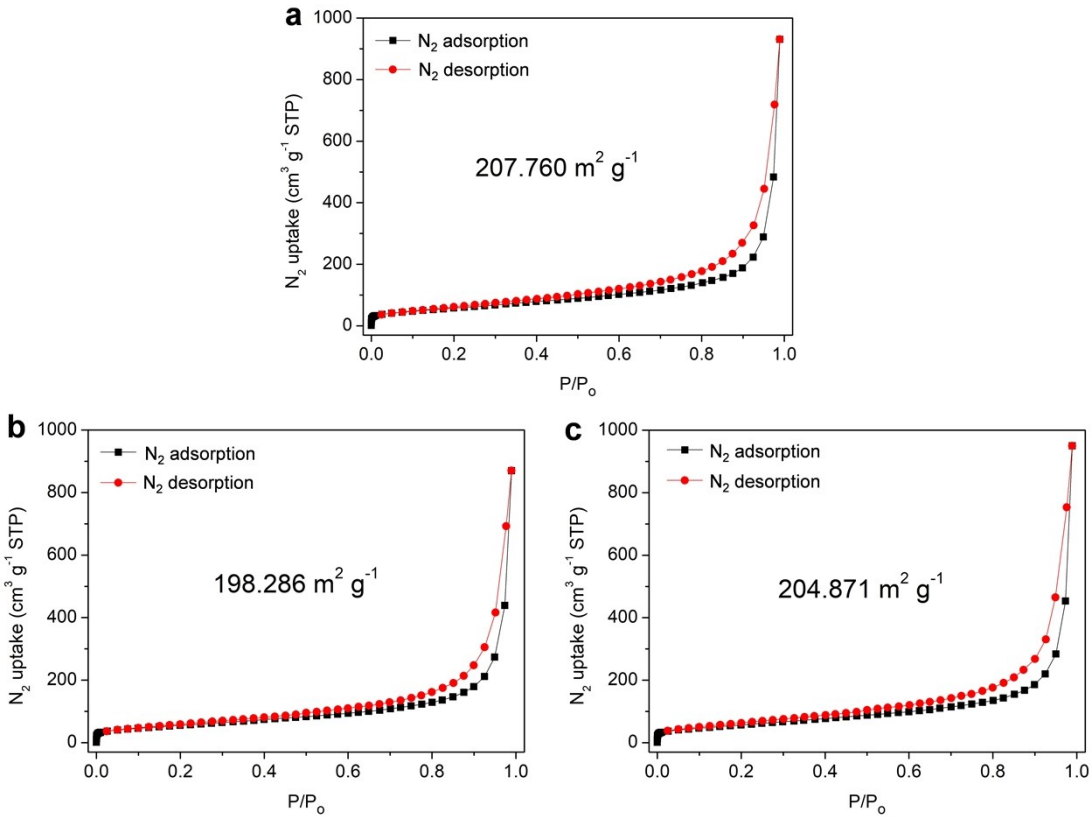

Supplementary Figure 14. Nitrogen adsorption-desorption isotherms for the Mo-CoOOH **(a)**, W-CoOOH **(b)**, and CoOOH **(c)**.

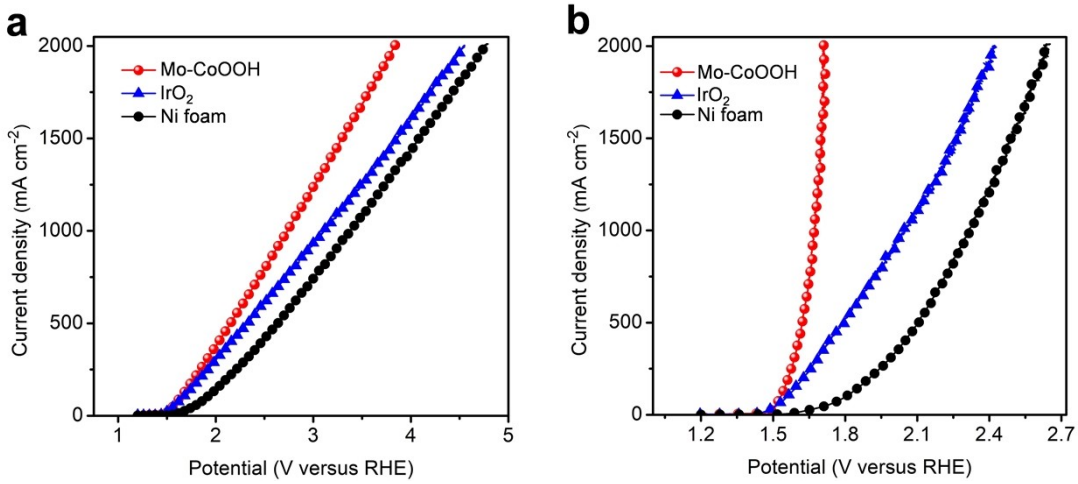

Supplementary Figure 15. The OER polarization curves for the Mo-CoOOH under large current densities in comparison with the IrO_2 and Ni foam, without iR corrections **(a)** and with 90% iR corrections **(b)**.

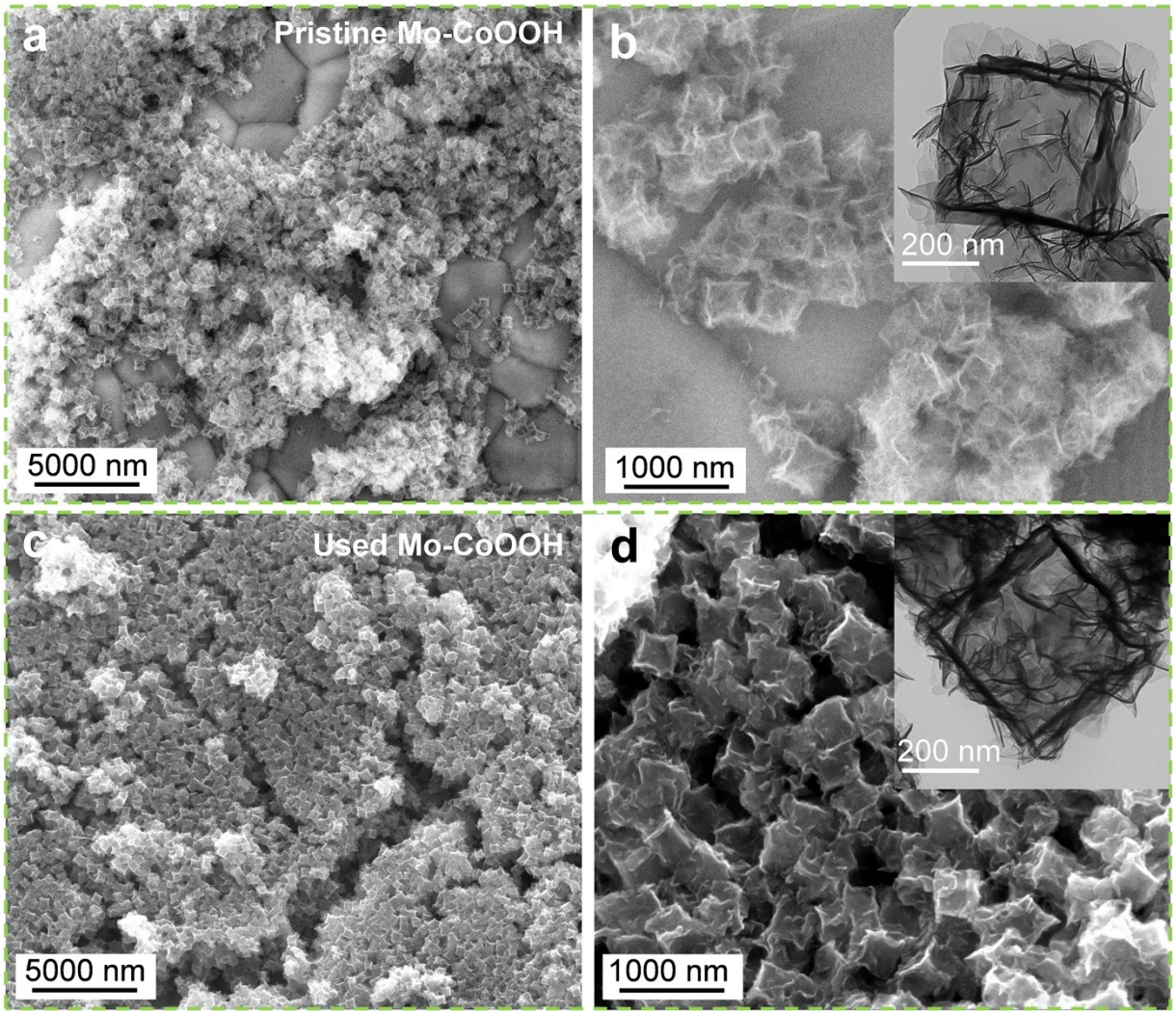

Supplementary Figure 16. Comparison of SEM and TEM images for the as-synthesized Mo-CoOOH sample **(a, b)** and that after OER stability test of 120 hours at 2000 mA cm^{-2} **(c, d)**, showing that the morphology of the nanoframes can be well maintained after the reaction.

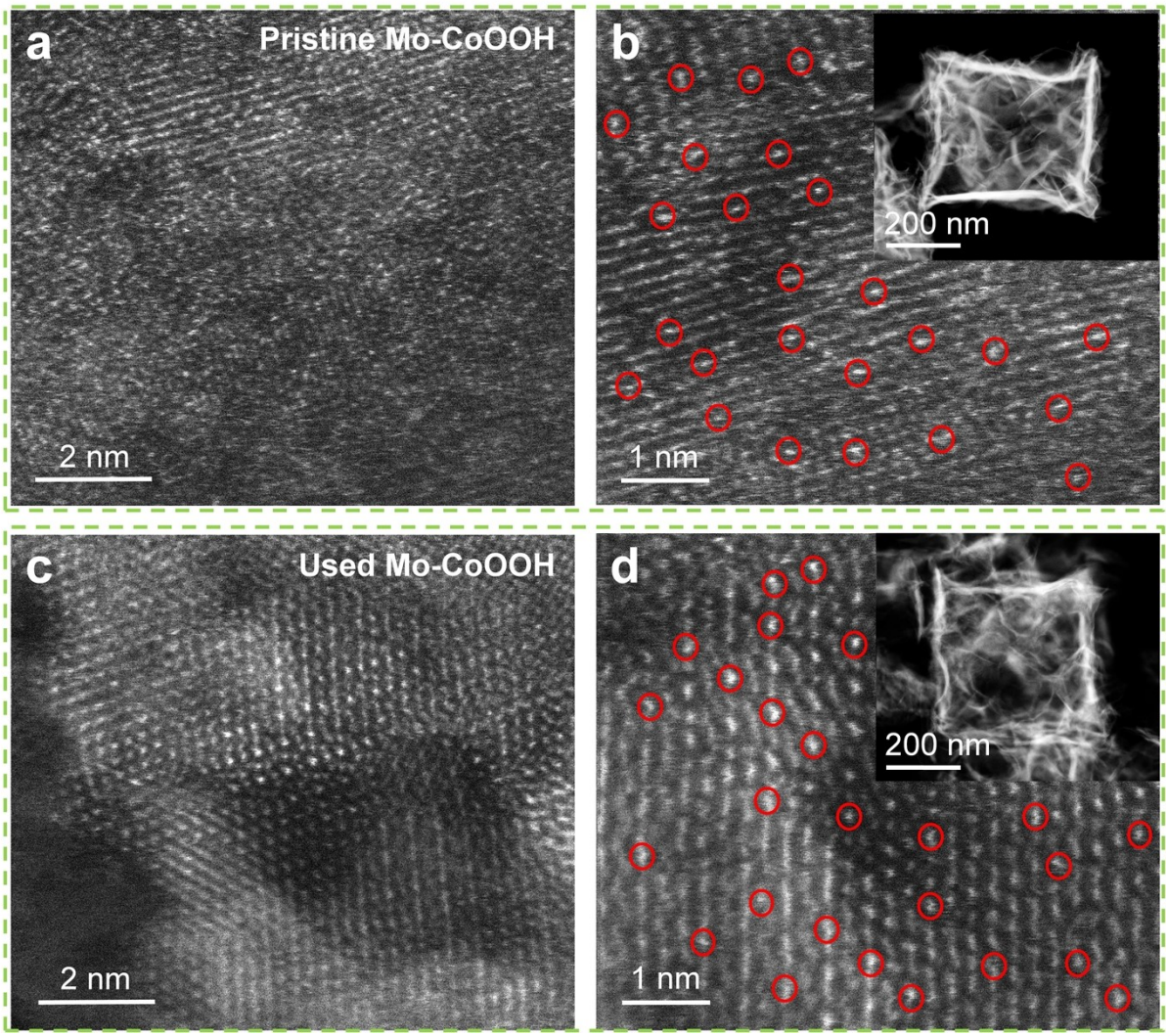

Supplementary Figure 17. Comparison of high-resolution HAADF-STEM images for the as-synthesized Mo-CoOOH sample **(a, b)** and that after OER stability test of 120 hours at 2000 mA cm^{-2} **(c, d)**, showing that the atomic structure of the Mo-CoOOH can be well maintained after the reaction.

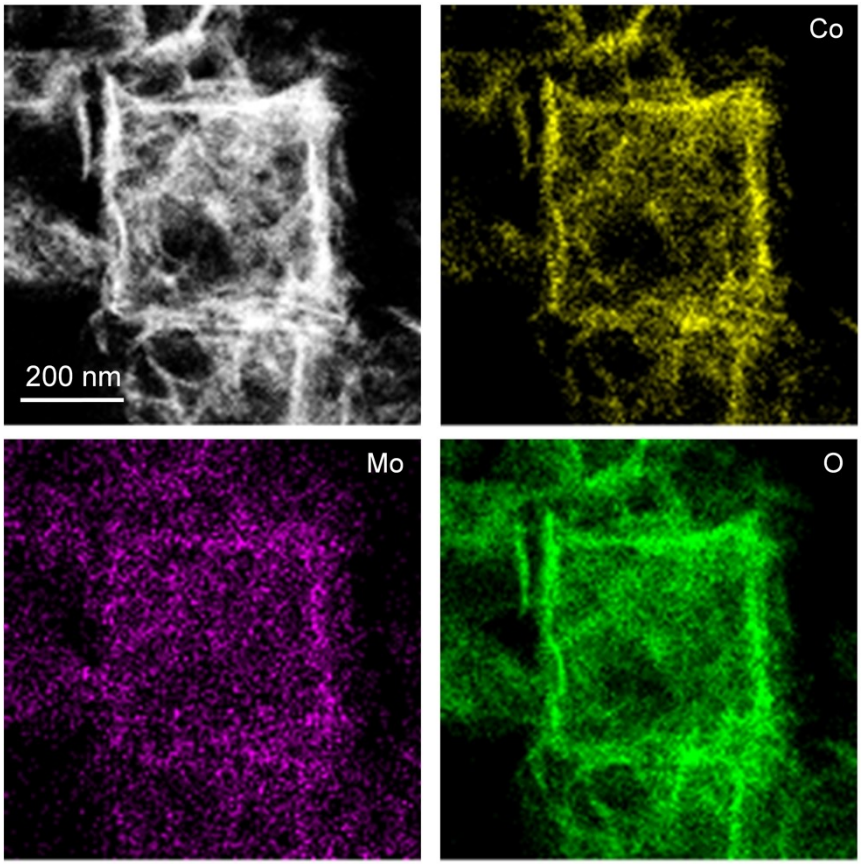

Supplementary Figure 18. EDS mapping of the Mo-CoOOH nanoframes after OER stability test of 120 hours at 2000 mA cm^{-2}.

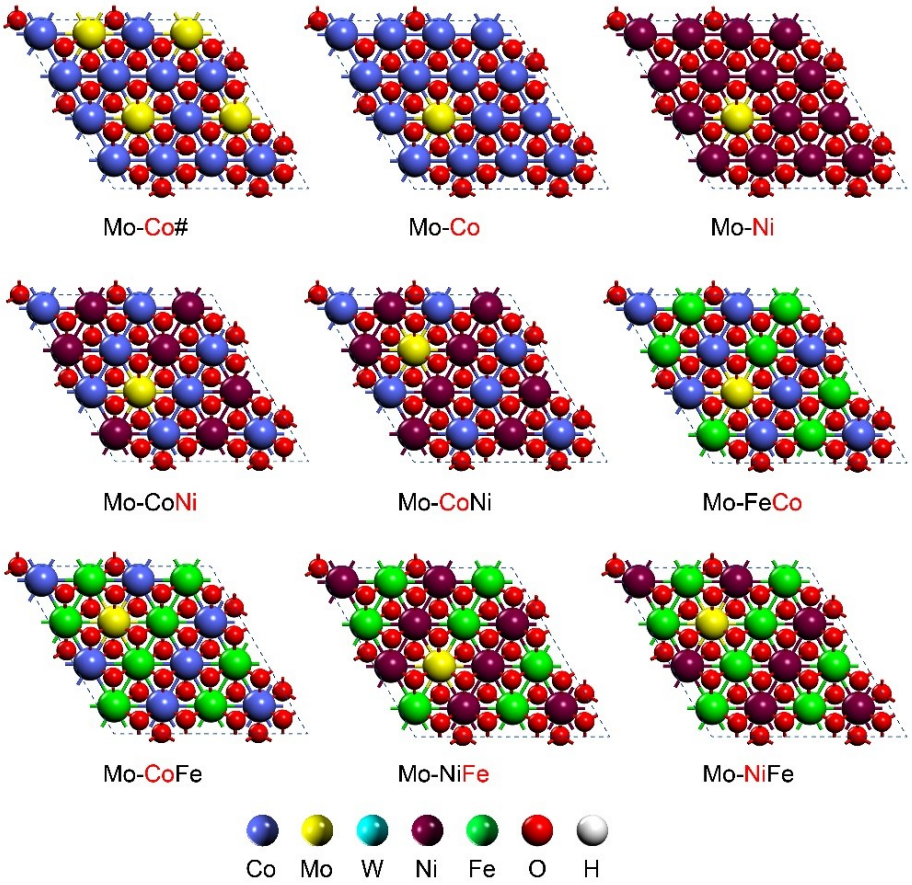

Supplementary Figure 19. Atomic structures of the CoOOH, NiOOH, CoNiOOH, CoFeOOH, and NiFeOOH confining Mo atoms, which are denoted as Mo-Co, Mo-Ni, Mo-CoNi, Mo-CoFe, and Mo-NiFe, respectively. The element symbols in red denote the elements that are replaced by Mo. The Co/Mo ratio is 3/1 in the Mo-Co#.

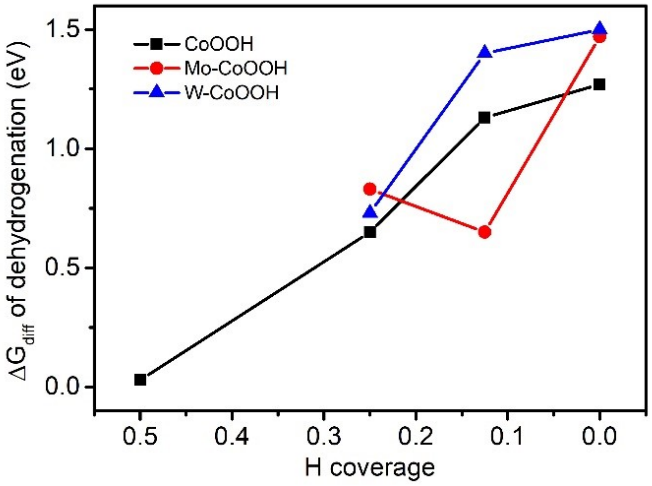

Supplementary Figure 20. The differential reaction free energy for the dehydrogenation of the CoOOH, Mo-CoOOH, and W-CoOOH, depending on the H coverage. The H coverage is defined as the number of H atoms divided by the number of O atoms in the supercell.

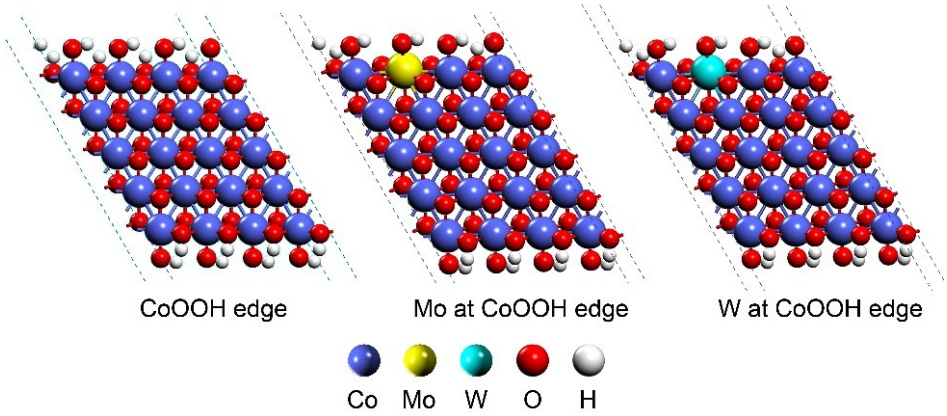

Supplementary Figure 21. Atomic structures of the pure, Mo-doped, and W-doped CoOOH edges.

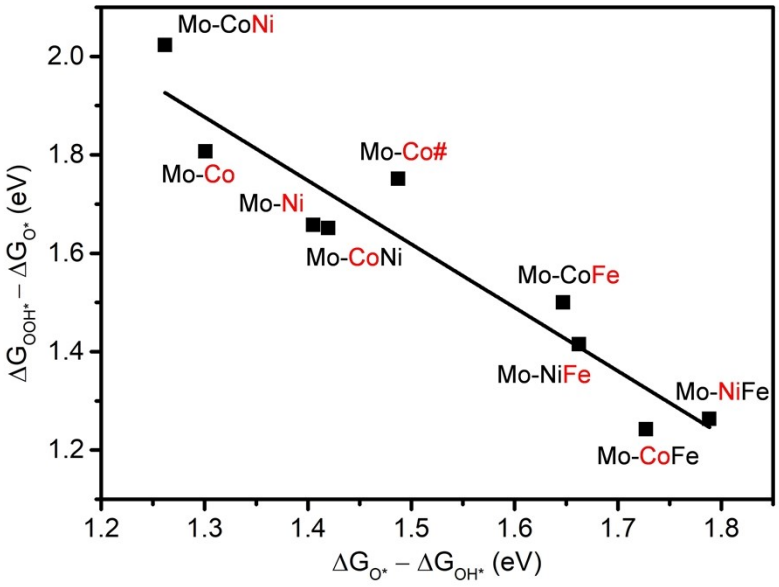

Supplementary Figure 22. The linear relation between the reaction free energies of the elementary steps (ii) and (iii).

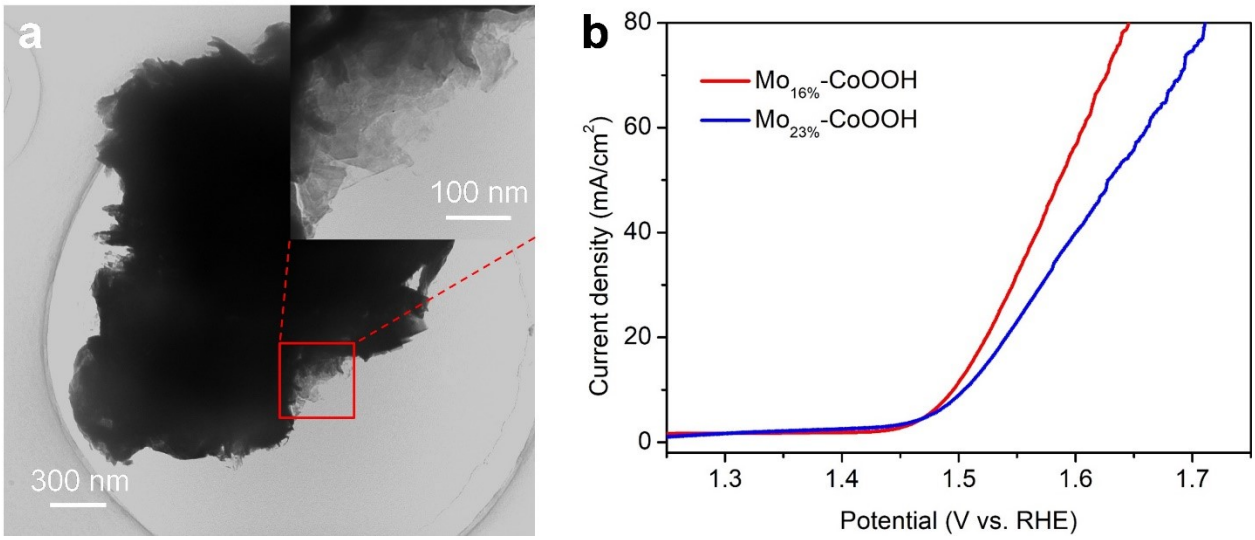

Supplementary Figure 23. (a) TEM images of the $Mo_{23\%}$-CoOOH. **(b)** The OER polarization curves of $Mo_{16\%}$-CoOOH and $Mo_{23\%}$-CoOOH catalysts loaded on glassy carbon electrode, without iR corrections.

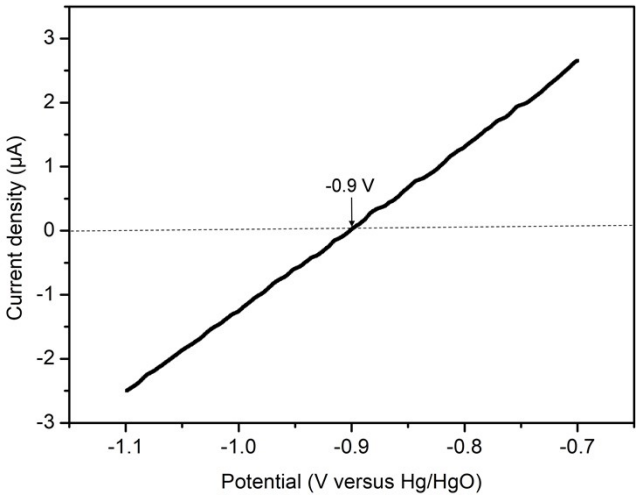

Supplementary Figure 24. The Hg/HgO reference electrode was calibrated in H_2-saturated 1 M KOH solution by measuring hydrogen oxidation/evolution on a platinum mesh electrode and defining the point of zero current as 0 V versus RHE. Therefore, $E_{RHE} = E_{Hg/HgO} + 0.9$ V.

4, Supplementary Table

Supplementary Table 1. Structural parameters of Mo with reference samples extracted from the Mo K-edge EXAFS fitting. (S_0^2= 0.9)[a].

Samples	Atomic scatter	CN[b]	Interatomic distance (Å)[c]	Debye-Waller factor (10^{-3}×Å^2)[d]	ΔE_0 (eV)[e]
Mo foil	Mo-Mo1	8	2.71	3.5	-6.8
	Mo-Mo2	6	3.13	3.0	-6.8
Mo-CoOOH	Mo-O	5.8	1.78	3.0	7.8

[a] S_0^2 was fixed as 0.9 during EXAFS fitting, based on the known structure of Mo foil. Error bounds that characterize the structural parameters obtained by EXAFS spectroscopy were estimated as N ± 20%.

[b] CN is the coordination number.

[c] Interatomic distance is the bond length between Mo central atoms and surrounding coordination atoms.

[d] Debye-Waller factor is a measure of thermal and static disorder in absorber-scattering distances.

[e] ΔE_0 is the difference between the zero kinetic energy value of the sample and that of the theoretical model.

Supplementary Table 2. Comparison in low-current-density OER activities of various layered transition-metal oxyhydroxides loaded on glassy carbon electrodes.

Catalyst	Electrolyte	Overpotential at 10 mA cm^{-2} (mV)	References
Mo-CoOOH	1 M KOH	249	This work
W-CoOOH	1 M KOH	330	This work
IrO_2	1 M KOH	290	This work
γ-CoOOH bulk	1 M KOH	374	*Angew. Chem. Int. Ed.* **54**, 8722-8727 (2015).
γ-CoOOH	1 M KOH	300	*Angew. Chem. Int. Ed.* **54**, 8722-8727 (2015).
Ultrathin FeCo LDH	1 M KOH	290	*Adv. Mater.* **29**, 1701546 (2017).
Ce-doped NiO_x	1 M NaOH	271	*Nat. Energy* **1**, 16053 (2016).
$Ni(OH)_2$−Au	1 M KOH	270	*J. Am. Chem. Soc.* **138**, 9128- 9136 (2016).
Au-NiFeOOH	1 M KOH	237	*J. Am. Chem. Soc.* **140**, 3876- 3879 (2018).
CoOOH	1 M KOH	300	*Nat. Mater.* **11**, 550-557 (2012).
$Li_{1-x}CoO_2$	0.1 M KOH	390	*J. Am. Chem. Soc.* **139**, 6270- 6276 (2017).
IrO_2	1 M KOH	330	*Angew. Chem. Int. Ed.* **54**, 8722-8727 (2015).
LDH NiFe	1 M KOH	300	*Nat. Commun.* **5**, 4477 (2014).
Fe 1 Co 1 -ONS Fe_1Co_1-ONS	0.1 M KOH	308	*Adv. Mater.* **29**, 1606793 (2017).
Mono-NiTi-MMO	1 M KOH	320	*J. Am. Chem. Soc.* **138**, 6517- 6524 (2016).

spinel $NiCo_2O_4$	1 M KOH	270	*J. Am. Chem. Soc.* **142**, 50-54 (2020).

Supplementary Table 3. Comparison in large-current-density OER activities of various catalysts loaded on Ni foam electrodes in 1 M KOH (N/A, not applicable).

Catalyst	Overpotential at 1000 mA cm^{-2} (mV)		Overpotential at 2000 mA cm^{-2} (mV)		References
	without iR correction	with iR correction	without iR correction	with iR correction	
Mo-CoOOH/Ni foam	1470	340	2570	400	This work
Ni microfiber felt	N/A	490	N/A	670	*Adv. Energy Mater.* 10, 2001174 (2020).
Ni-Cu nanowire felt	N/A	600	N/A	770	*Adv. Energy Mater.* 10, 2001174 (2020).
3D-O_2-Cat-1	670	340	N/A	N/A	*Nat. Commun.* 9, 2609 (2018).
3D-O_2-Cat-2	1520	380	N/A	N/A	*Nat. Commun.* 9, 2609 (2018).
Fe_2O_3@Ni_2P/Ni$(PO_3)_2$/Ni foam	770	370	N/A	N/A	*J. Mater. Chem. A* 7, 965-971 (2019).
Sn-Ni_3S_2/Ni foam	1480	570	N/A	N/A	*ACS Appl. Mater. Interfaces* 10, 40568-40576 (2018).

5, Supplementary References:

1. Blochl, P.E. Projector augmented-wave method. *Physical Review B* **50**, 17953-17979 (1994).
2. Kresse, G. & Furthmuller, J. Efficiency of ab-initio total energy calculations for metals and semiconductors using a plane-wave basis set. *Computational Materials Science* **6**, 15-50 (1996).
3. Kresse, G. & Furthmuller, J. Efficient iterative schemes for ab initio total-energy calculations using a plane-wave basis set. *Physical Review B* **54**, 11169-11186 (1996).
4. Kresse, G. & Hafner, J. Ab initio molecular dynamics for liquid metals. *Physical Review B* **47**, 558-561 (1993).
5. Kresse, G. & Hafner, J. Ab initio molecular-dynamics simulation of the liquid-metal–amorphous-semiconductor transition in germanium. *Physical Review B* **49**, 14251-14269 (1994).
6. Kresse, G. & Joubert, D. From ultrasoft pseudopotentials to the projector augmented-wave method. *Physical Review B* **59**, 1758-1775 (1999).
7. Perdew, J.P., Burke, K. & Ernzerhof, M. Generalized gradient approximation made simple. *Physical Review Letters* **77**, 3865-3868 (1996).
8. Perdew, J.P., Burke, K. & Ernzerhof, M. Generalized gradient approximation made simple (vol 77, pg 3865, 1996). *Physical Review Letters* **78**, 1396-1396 (1997).
9. Grimme, S., Antony, J., Ehrlich, S. & Krieg, H. A consistent and accurate ab initio parametrization of density functional dispersion correction (DFT-D) for the 94 elements H-Pu. *Journal of Chemical Physics* **132**, 154104 (2010).
10. Grimme, S., Ehrlich, S. & Goerigk, L. Effect of the damping function in dispersion corrected density functional theory. *Journal of Computational Chemistry* **32**, 1456-1465 (2011).
11. Monkhorst, H.J. & Pack, J.D. Special points for brillouin-zone integrations. *Physical Review B* **13**, 5188-5192 (1976).
12. Gao, M. et al. Efficient water oxidation using nanostructured alpha-Nickel-Hydroxide as an electrocatalyst. *Journal of the American Chemical Society* **136**, 7077-7084 (2014).